

Contents lists available at ScienceDirect

### Journal of Rock Mechanics and Geotechnical Engineering

journal homepage: www.jrmge.cn



Full Length Article

## Undrained shear strength of biochar-assisted biocemented calcareous sand by biostimulated microbially induced calcium carbonate precipitation



Yijie Wang <sup>a, b</sup>, Xiaole Han <sup>c</sup>, Kaiwei Liu <sup>d</sup>, Juan Du <sup>e</sup>, Wenbo Chen <sup>f</sup>, Zhenyu Yin <sup>g</sup>, Shu Yu <sup>a</sup>, Ningiun Jiang <sup>b, \*</sup>

- <sup>a</sup> State Key Laboratory of Simulation and Regulation of Water Cycle in River Basin, China Institute of Water Resources and Hydropower Research, Beijing, 100048. China
- <sup>b</sup> Institute of Geotechnical Engineering, Southeast University, Nanjing, 211189, China
- <sup>c</sup> Department of Civil and Environmental Engineering, University of Hawaii at Manoa, Honolulu, 96822, USA
- <sup>d</sup> Anhui Provincial Key Laboratory of Advanced Civil Engineering Material, Anhui Jianzhu University, Hefei, 230601, China
- <sup>e</sup> School of Civil Engineering and Architecture, Hainan University, Haikou, 570228, China
- <sup>f</sup> College of Civil and Transportation Engineering, Shenzhen University, Shenzhen, 518060, China
- g Department of Civil and Environmental Engineering, The Hong Kong Polytechnic University, Hong Kong, China

#### ARTICLE INFO

# Article history: Received 24 June 2024 Received in revised form 8 September 2024 Accepted 24 November 2024 Available online 15 December 2024

Keywords:
Biostimulation
Biochar
Triaxial consolidated undrained (CU) shear
test
Ureolytic activity
Failure criterion

#### ABSTRACT

Biostimulation has been proven to be an available approach for microbially induced calcium carbonate precipitation (MICP). However, biostimulation may not be as effective as bioaugmentation in some unfavorable situations. In this study, the feasibility of biochar-assisted MICP for improving the shear strength of calcareous sand is investigated. The optimization of cementation solution for biostimulated MICP is first determined through a series of unconfined compressive tests. The shear characteristics of biocemented calcareous sand, enhanced by biochar and treated through biostimulation, are then assessed using consolidated undrained (CU) shear triaxial tests. To characterize the shear strength of biocemented sand under low effective normal stress, both Mohr-Coulomb failure envelopes and nonlinear failure envelopes were employed. Meanwhile, the current study also compared and analyzed two distinct stress states: maximum principal stress ratio  $((\sigma'_1/\sigma'_3)_{max})$  and Skempton's pore pressure parameter  $\overline{A} = 0$ , to identify an appropriate failure criterion for determination of the shear strength parameters. Furthermore, the microscopic features and post-failure characteristics of biochar-assisted calcareous sand were examined and discussed. The findings indicate that biochar can contribute to an increase in cementation content by serving as additional nucleation sites. The study may provide valuable insights into the potential of biochar-assisted MICP for enhancing the biostimulation approach. © 2025 Institute of Rock and Soil Mechanics, Chinese Academy of Sciences. Published by Elsevier B.V. This is an open access article under the CC BY-NC-ND license (http://creativecommons.org/licenses/by-nc-nd/ 4.0/).

#### 1. Introduction

Ureolysis-based microbially induced calcium carbonate precipitation (MICP) is a process in which microorganisms are used to facilitate precipitation of the calcium carbonate. It shows that certain types of bacteria, such as Bacillus species, are particularly effective at inducing calcium carbonate precipitation, and that factors such as temperature, pH, and nutrient availability can affect

Bioaugmentation and biostimulation are two approaches that can be used to enhance the MICP (Gomez et al., 2017). Bioaugmentation involves introduction of the specific microorganisms, such as bacteria or fungi, into a system to promote the

the process (Tang et al., 2020; Wang et al., 2020; Lai et al., 2021a; Xiao et al., 2021). By optimizing these conditions, researchers have been working to improve the efficiency and effectiveness of MICP for various applications. This process has attracted a lot of attention in recent years due to its potential applications in a wide range of geo-environmental fields, such as construction (Vekariya and Pitroda, 2013), bioremediation (Mwandira et al., 2017; Jiang et al., 2019), and soil stabilization (Jiang et al., 2022).

<sup>\*</sup> Corresponding author. E-mail address: jiangn@seu.edu.cn (N. Jiang).

precipitation of calcium carbonate. The introduced microorganisms are typically selected for their ability to produce urease that can interact with urea and further initiate the precipitation process. This approach can be effective when the natural microbial community is not capable of producing enough calcium carbonate or the specific environmental conditions favor the growth of introduced microorganisms. Biostimulation, on the other hand, involves providing nutrients or other growth-promoting factors to the existing microbial community to enhance their ability to precipitate calcium carbonate (Gat et al., 2016; Wang et al., 2023a). This approach aims to stimulate the growth and activity of native microorganisms, which can be more cost-effective and sustainable than introducing new microorganisms. It can be achieved by adding nutrients such as nitrogen and carbon sources to the system, and by manipulating some critical environmental factors such as temperature or pH, which leverages the existing microbial community. Normally, biostimulation can be achieved by adding relatively inexpensive nutrients or adjusting environmental factors (Gowthaman et al., 2019; Pakbaz et al., 2020). However, it should be noted that biostimulation may not be as effective as bioaugmentation in certain situations, such as when the native microbial community is not capable of producing enough calcium carbonate due to the initial low concentration or when specific environmental conditions do not favor the growth of native microorganisms.

To overcome the above-mentioned potential inapplicable situation of biostimulation method, amending the biostimulated MICP process with decent auxiliary additives to improve the efficiency might be a practicable way. Biochar is a carbon-rich material that is produced by pyrolysis of organic matter, such as agricultural waste or forestry residues. It has been shown to have a range of beneficial effects on soil properties, including improving soil fertility, water retention, and nutrient cycling (Chan et al., 2007; Verheijen et al., 2010). In the context of MICP, it is believed that biochar could potentially act as a substrate for microorganisms, providing a source of nutrients and a stable carbon source for microbial growth. It could also improve the physical properties of the soil, such as porosity and water retention, which could enhance the effectiveness of the biostimulated MICP process. Furthermore, Biochar may provide a favorable habitat for microorganisms, with its porous structure providing spaces for microbial colonization and growth (Kolb et al., 2009). This can help to enhance the activity and diversity of the microbial community, and thus improve the effectiveness of biostimulation. To the authors' knowledge, there are very limited studies regarding the biochar-assisted biostimulated MICP process.

Calcareous sand is a type of soil composed of mostly calcium carbonate particles. This type of soil can be problematic for construction projects due to its low shear strength and susceptibility to break especially in the tropical regions. Brandes (2011) found that particle breakage and rounding of Hawaiian calcareous sand under higher normal stress during shearing can cause a substantial decrease in friction angle using direct simple shear test. This decrease was more severe in calcareous sand compared with silica sand due to its low grain hardness and more prevalent intraparticle voids. Biostimulated MICP method shows great potentials in enhancing calcareous sands by forming interparticle cementation. Khan et al. (2015) and Liu et al., (2018, 2019), evaluated the feasibility of MICP to solidify calcareous sand. However, their mechanical investigations were limited to bioaugmentation process under the tests of unconfined compressive strength (UCS) and triaxial consolidated drained strength. The behavior of saturated biocemented sand in the situation where pore water pressure does not have time to dissipate still requires further investigation.

The process flow diagram of the current study is displayed in

Fig. 1. In detail, the recipe optimization investigations of cementation solution for biostimulated MICP process is firstly determined by a series of unconfined compressive tests. Although some scholars have conducted research on the optimal concentration of the cementing solution in bioaugmented MICP process (e.g. Mujah et al., 2019; Lai et al., 2021b), the study on this aspect of biostimulated MICP is still incomplete. Subsequently, the influence of biochar on ureolytic activity was examined to determine its beneficial role in the biostimulation process under aqueous conditions. Following this, the shear characteristics of biocemented calcareous sand, enhanced by biochar and treated through biostimulation, were assessed using a series of consolidated undrained (CU) triaxial shear tests under varying confining pressures. Experimental evidences indicate that the Mohr envelopes of numerous soils are nonlinear, particularly within the range of low effective normal stresses (e.g. Maksimovic, 1989). To characterize the shear strength of biocemented sand more accurately under low effective normal stress, both Mohr-Coulomb failure envelopes and nonlinear failure envelopes, as proposed by Baker (2004), are employed to evaluate the shear strength of biochar-assisted biocemented sands. Moreover, two distinct stress states, maximum principal stress ratio  $((\sigma'_1/\sigma'_3)_{
m max})$ , and Skempton's pore pressure parameter  $\overline{A}=0$ , are compared and analyzed to identify an appropriate failure criterion. This enables engineers and researchers to precisely predict the mechanical behavior of biocemented sand. In addition, the microscopic features and post-failure characteristics of biochar-assisted biocemented calcareous sand were discussed.

#### 2. Materials and methods

#### 2.1. Sand and biochar

In this study, calcareous sand was collected from supratidal zone of Kahanamoku Beach, located on Oahu Island, Hawaii, USA. The particle size distribution of surface sand, sampled up to a depth of 3 cm, is shown in Fig. 2. Prior to testing, the sand was sieved through a 2 mm aperture sieve to eliminate oversized grains, and extraneous materials such as small twigs, grass, and microplastic particles were removed. The physical properties of the calcareous sand are provided in Table 1.

The biochar employed in this study was procured from Pacific

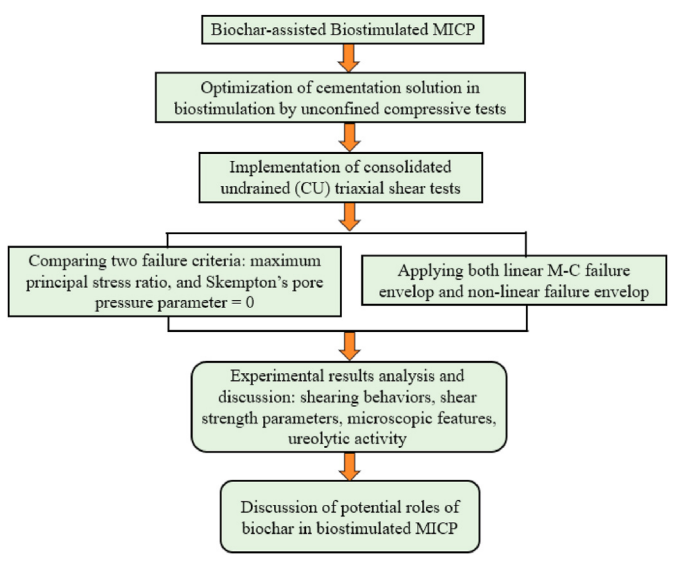


Fig. 1. The process flow diagram of the current study.

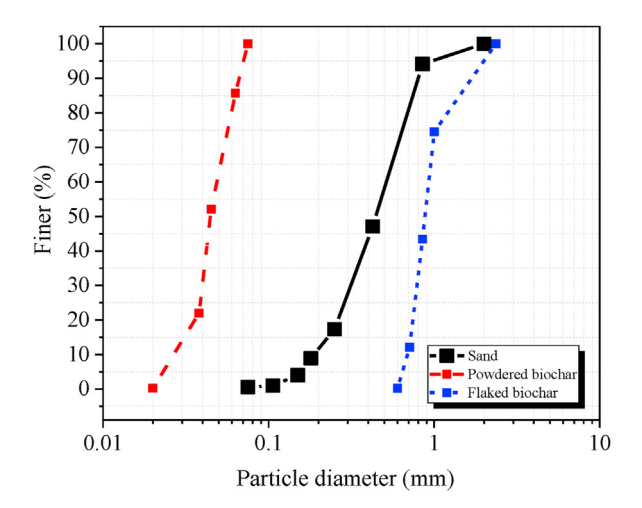


Fig. 2. Particle size distribution curves of sand, powdered biochar, and flaked biochar.

**Table 1**The physical properties of the collected calcareous sand.

Physical and Index Properties	Unit	Value
Soil classification (ASTM D2487)		SP (poorly-graded clean sand)
Median particle diameter, $D_{50}$	mm	0.360
Coefficient of curvature $C_c$		0.816
Coefficient of uniformity $C_u$		2.5
Maximum void ratio $e_{max}$		0.888
Minimum void ratio $e_{\min}$		0.271
Carbonate content	%	≥99.5
Natural moisture content		1-1.5
Average circularity		0.826
Average aspect ratio		1.511

Biochar (Santa Rosa, CA) and produced from softwood forestry residues. The biochar exhibited a bulk density of 155.8 kg/m³, a cation exchange capacity of 21.5 meq/(100 g), and a butane activity of 7%. The pH value of biochar was around  $9.0 \pm 0.2$ . Table 2 displays the chemical composition of the biochar. Two distinct biochar shapes were utilized in this research. The first type, a powder-like biochar, had a particle size of less than 0.075 mm and was obtained by passing the material through a US No. 325 sieve to remove oversized particles. The second type, the flaked biochar, featured particle size larger than 0.6 mm and was acquired by sieving to retain particles on a US No. 20 sieve. Fig. 2 presents the particle size distribution curves of these two biochar types.

#### 2.2. Biostimulation process

In this study, we employed an enrichment medium comprising 20 g/L yeast extract (YE) and 10.21 g/L urea (170 mM) (1 M = 1 mol/

**Table 2**Chemical content of biochar in percentage.

Ingredient	Content (%)
N	0.1
P	0.08
$P_2O_5$	0.18
K	0.39
K <sub>2</sub> O	0.47
S	0.03
Ca	0.6
Mg	0.1
Na	0.04
C	>85
Ash	4-8

L), which has been demonstrated to effectively enrich indigenous ureolytic bacteria (Wang et al., 2020, 2022a, 2023b). The YE, nutrient rich in proteins, amino acids, trace elements, and growth factors, was utilized as the organic nutrient to support bacterial growth, while urea functioned as a selective substrate to promote the enrichment of indigenous ureolytic bacteria. The cementation solution contained equal molar concentrations of urea and CaCl<sub>2</sub> (0.5 M), supplemented with 0.2 g/L YE to maintain bacterial viability throughout the cementation phase.

In cylindrical sand column condition, specimens were prepared using a PVC split mold with a height of 10 cm and an inner diameter of 5 cm. A total of 330 g of fresh calcareous sand and 0.99 g (0.3% weight ratio to sand) of air-dried biochar were uniformly combined in a stainless-steel container. The mixture was poured into the PVC split mold employing the dry pluviation method in three layers and compacted to achieve a relative density of 55.2%-57.9% with a dry density around (1.77  $\pm$  0.01) g/cm<sup>3</sup>. While the marginal difference has a small effect on the mixed soil density, the addition of biochar (either flakes or powders) itself (even very small amounts) may still influence the soil matrix fabrics and shearing behaviors. This requires further experimental investigation. The biostimulated MICP treatment comprised two phases: enrichment and cementation. To initiate the enrichment phase, the sample was flushed with one pore volume (PV) of enrichment medium (75 mL) using a peristaltic pump via surface percolation at room temperature (20  $\pm$  0.5) °C. The flow rate was maintained at 2 mL/min without disturbing the specimens, as previously reported in our research (Wang et al., 2022a). The specimens were then allowed to enrich for 48 h. Upon completion of the enrichment phase, the cementation phase commenced. The specimens were flushed with 1.5 PVs (112.5 mL) of cementation solution through surface percolation at a flow rate of 2 mL/min for either 4 or 10 consecutive days, resulting in specimens with varying cementation contents. Subsequently, all specimens were flushed with 3 PVs (225 mL) of deionized water five times to eliminate any residual dissolved salts before being airdried. It should be noted that the specimens were not subjected to external loads during either the enrichment or cementation phase.

The effects of biochar on ureolytic activity of biostimulation process was investigated in solution condition, where only the enrichment phase was carried out by mixing the collected calcareous sand with enrichment media in sterilized Erlenmeyer flasks (500 mL) with air-permeable cap to facilitate air circulation. In each flask, 20 g of fresh sand was combined with either 150 mL of enrichment media and 2 g of biochar, or 300 mL of enrichment media and 4 g of biochar. The biochar mass to enrichment medium volume ratio was maintained at approximately 1:75, which was consistent with the ratio observed in the sand column condition under saturation situation. Triplicate samples were prepared to ensure the reliability of the results. The centrifuge tubes were then placed into a shaking incubator, and the experiment was conducted at 200 r/min (acceleration of 0.425g) and 30 °C for 72 h. During the experiment, ureolytic activity was assessed at specified intervals over a period of 108 h.

### 2.3. Unconfined compressive test and triaxial consolidated undrained test

Upon completion of the biostimulated MICP treatment, cylindrical sand specimens were subjected to unconfined compression tests based on ASTM D2166M (2016) and CU triaxial compression tests in accordance with ASTM D4767-11 (2020), respectively. In the unconfined compression test, the specimens were loaded axially at an axial strain rate of 1.5 %/min, and the maximum load per unit area was chosen as the unconfined compressive strength ( $q_u$ ). In the

 Table 3

 Characteristics of unconfined compressive test specimens.

Specimen	Duration of cementation phase (d)	Initial D <sub>r</sub> (%)	Ca <sup>2+</sup> /urea concentration (M)
A1	2	55.4	0.1
A2		56.1	0.5
A3		56.8	1.0
B1	4	57.2	0.1
B2		58.3	0.5
B3		55.8	0.1.0
C1	10	57.1	0.1
C2		57.6	0.5
C3		56.8	1.0

CU triaxial test, saturation was achieved by applying back pressure to the specimen. During back pressuring, the difference between the chamber pressure and the back pressure was 25 kPa. Specimens were considered saturated if the value of parameter *B*-value was equal to or greater than 0.95. A strain rate of 1%/h was applied. The characteristics of specimens subjected to unconfined compressive tests and CU triaxial tests are presented in Tables 3 and 4, respectively.

#### 2.4. Measurement of ureolytic activity

The ureolytic activity (mM/mL min) was measured and calculated using an ultraviolet (UV) spectrophotometer. A 1 mL aliquot of the bacterial solution was mixed with 1.5 M urea and subsequently diluted to the desired concentration. Following a 5-min reaction, the increase in ammonium concentration of the above-mentioned diluted mixture was determined by measuring absorbance at a wavelength of 425 nm using a spectrophotometer (Knorst et al., 1997). In detail, 2 mL of the collected diluted mixture solution, obtained after filtrating by 0.45  $\mu m$  filter paper, was mixed with 0.1 mL of Nessler's reagent and allowed to react for 10 min before reading the absorbance value. The relationship between the absorbance at 425 nm (OD425) and the ammonium concentration was established using a pre-made reference curve, as demonstrated in Eq. (1).

Ammonium concentration (mM) = 
$$OD_{425} / 0.489$$
 (1)

#### 3. Results

#### 3.1. Optimization of biostimulated MICP treatment

The optimization of the cementation solution for the biostimulated MICP process is initially determined through a series of unconfined compressive tests. The cementation content (*CC*) is firstly determined by measuring the mass change before and after biostimulated MICP treatment, which can be expressed as

$$CC = \frac{m_{at} - m_{bt} - m_B}{m_{bt}} \times 100\%$$
 (2)

where  $m_{bt}$  is the dry mass of specimen prior to MICP treatment,  $m_{at}$  is the dry mass of specimen after MICP treatment, and  $m_B$  is the dry mass of added biochar.

The variations in *CC* corresponding to different durations of the cementation period and concentration of cementation solution are depicted in Fig. 3a. It is evident that for a fixed concentration of cementation solution, the *CC* increased as the treatment duration is extended. Specifically, for specimens treated with 0.1 M cementation solution, the *CC* exhibited an approximate 44% and 80% increment for the 4-d and 10-d samples, respectively, in comparison to the 2-d samples. In the case of samples treated with 0.5 M cementation solution, the *CC* experienced an approximate 184% and 300% enhancement for the 4-d and 10-d samples, respectively, relative to the 2-d samples. Lastly, for specimens treated with 1 M cementation solution, the *CC* demonstrated an approximate 129% and 168% escalation for the 4-d and 10-d samples, respectively, compared to the 2-d samples. However, the rate of *CC* increased

**Table 4** Characteristics of triaxial consolidated undrained test specimens.

Specimen nomenclature	Initial $D_{\rm r}$ (%)	Duration of cementation phase (d)	Biochar content by weight (%)	Biochar type	Confining pressure (kPa)	Average $q_{\mathrm{u}}$ (kPa)
Untreated	55.2	N/A	0	N/A	50	0
Untreated	56.5	N/A	0	N/A	100	
Untreated	55.9	N/A	0	N/A	200	
Untreated	57.1	N/A	0	N/A	400	
Bio_L	56.6	4	0	N/A	50	174.6
Bio_L	55.6	4	0	N/A	100	
Bio_L	57.9	4	0	N/A	200	
Bio_L	57.8	4	0	N/A	400	
Bio_H	57.4	10	0	N/A	50	782.6
Bio_H	56.4	10	0	N/A	100	
Bio_H	55.4	10	0	N/A	200	
Bio_H	0.56.5	10	0	N/A	400	
Bio_B(F)	. 57.1	10	0.3	Flake (F)	50	651.9
Bio_B(F)	. 56.2	10	0.3	Flake (F)	100	
Bio_B(F)	. 56.2	10	0.3	Flake (F)	200	
Bio_B(F)	0.55.7	10	0.3	Flake (F)	400	
Bio_B(P)	. 57.4	10	0.3	Powder (P)	50	962.1
Bio_B(P)	. 56.8	10	0.3	Powder (P)	100	
Bio_B(P)	. 56.7	10	0.3	Powder (P)	200	
Bio_B(P)	. 55.9	10	0.3	Powder (P)	400	

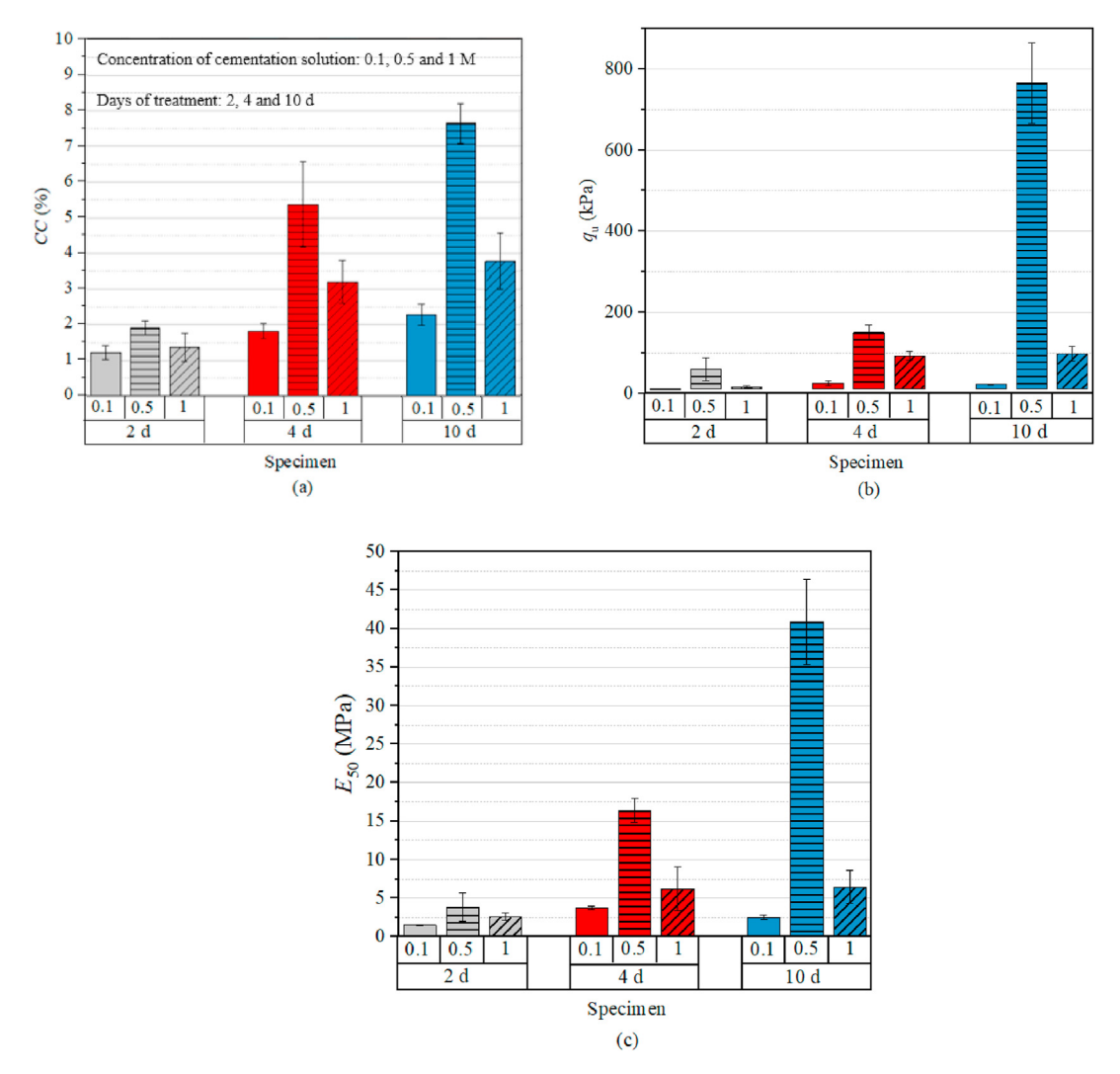


Fig. 3. Various key parameters of tested specimens: (a) The cementation content, (b) the unconfined compressive strength, and (c) the secant stiffness.

diminishes over time, which may be attributed to either the reduced availability of voids for CaCO<sub>3</sub> deposition or the decline in ureolytic bacteria due to the multiple flushes. For a fixed treatment duration period, it was apparent that the samples treated with 0.1 M cementation solution exhibited the lowest *CC*, followed by

1 M, while the 0.5 M concentration displayed the highest *CC* content. Specifically, for 2-d specimens, the *CC* content increased by approximately 57% and 12% for concentrations of 0.5 M and 1 M, respectively, compared to 0.1 M. For 4-d specimens, the *CC* experienced an approximate 195% and 76% increment for

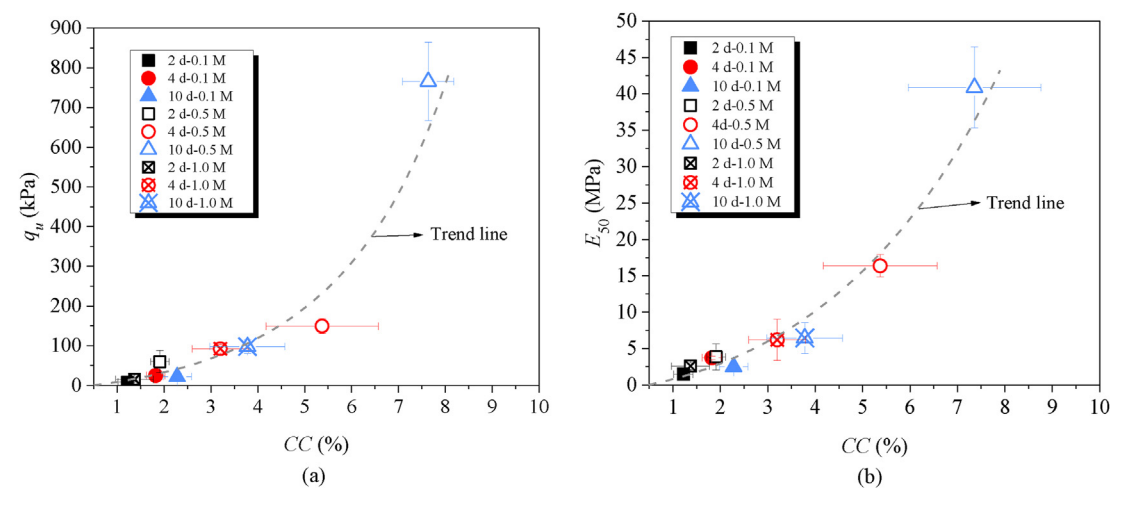
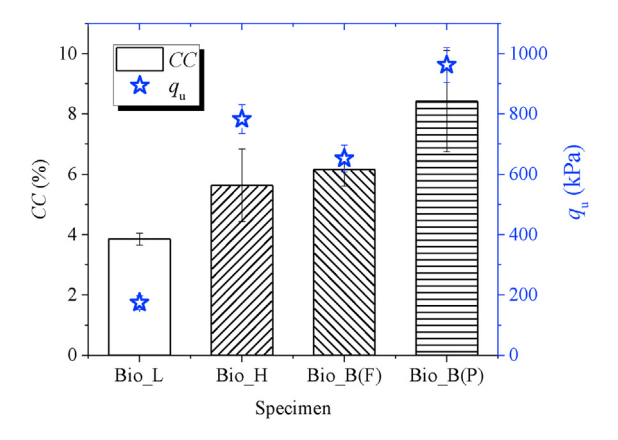


Fig. 4. The relationship between cementation content and unconfined compressive strength and secant stiffness.



**Fig. 5.** Cementation content and unconfined compressive strength of biochar-assisted and non-biochar-assisted biocemented specimen.

concentrations of 0.5 M and 1 M, respectively. For 10-d samples, the CC demonstrated an approximate 235% and 66% enhancement for concentrations of 0.5 M and 1 M, respectively. In addition, the unconfined compressive strength ( $q_{\rm u}$ ) and secant stiffness ( $E_{50}$ ) showed very similar trends as CC corresponding to different durations of the cementation period, and concentration of cementation solution. It was found that  $q_{\rm u}$  and  $E_{50}$  generally increased with longer cementation stage at a given cementation solution concentration (i.e. 0.1 M, 0.5 M, or 1 M). For a fixed treatment number of times, the highest values of  $q_{\rm u}$  and  $E_{50}$  were observed at a cementation solution concentration of 0.5 M, as illustrated in

Fig. 3b and c, in comparison to the results obtained at either 0.1 M or 1 M concentrations. Furthermore, the relationships between  $q_{\rm u}$  and  $E_{50}$  are illustrated in Fig. 4a and b. In general, as the CC increased, both  $q_{\rm u}$  and  $E_{50}$  exhibited a corresponding increase, irrespective of the variations in cementation stage duration and cementation solution concentration, which was consistent with some previous studies (Montoya and DeJong, 2015; Gomez et al., 2015). The increase in  $q_{\rm u}$  and  $E_{50}$  was attributed to the formation of calcite bonds between the sand grains, which enhanced the interparticle forces and creates a more rigid structure.

These observations could be due to the distinct morphologies of the generated CaCO<sub>3</sub> crystals at varying cementation solution concentrations. Burdalski and Gomez (2020) examined the impact of different Ca<sup>2+</sup> concentrations in cementation solution on the morphology of CaCO<sub>3</sub> under bioaugmentation treatment. At a concentration of 0.5 M (equal concentrations of urea and CaCl<sub>2</sub>), the sample exhibited a predominantly calcite phase (96%) with minimal amounts (approximately 2%) of vaterite and aragonite. When the concentration increased to 1250 mM, calcite remained the dominant phase (75%), while the proportion of vaterite significantly rose to 23%. Calcite has the most stable polymorph of calcium carbonate with a trigonal crystal system. Conversely, vaterite, the least stable polymorph of calcium carbonate, possesses a hexagonal crystal system. Aragonite, a metastable polymorph of calcium carbonate, is characterized by its intermediate stability between calcite and vaterite. Consequently, a higher percentage of calcite in the context of a 0.5 M cementation solution may contribute to an increase in unconfined compressive strength and stiffness. Furthermore. Soon et al. (2014) investigated the

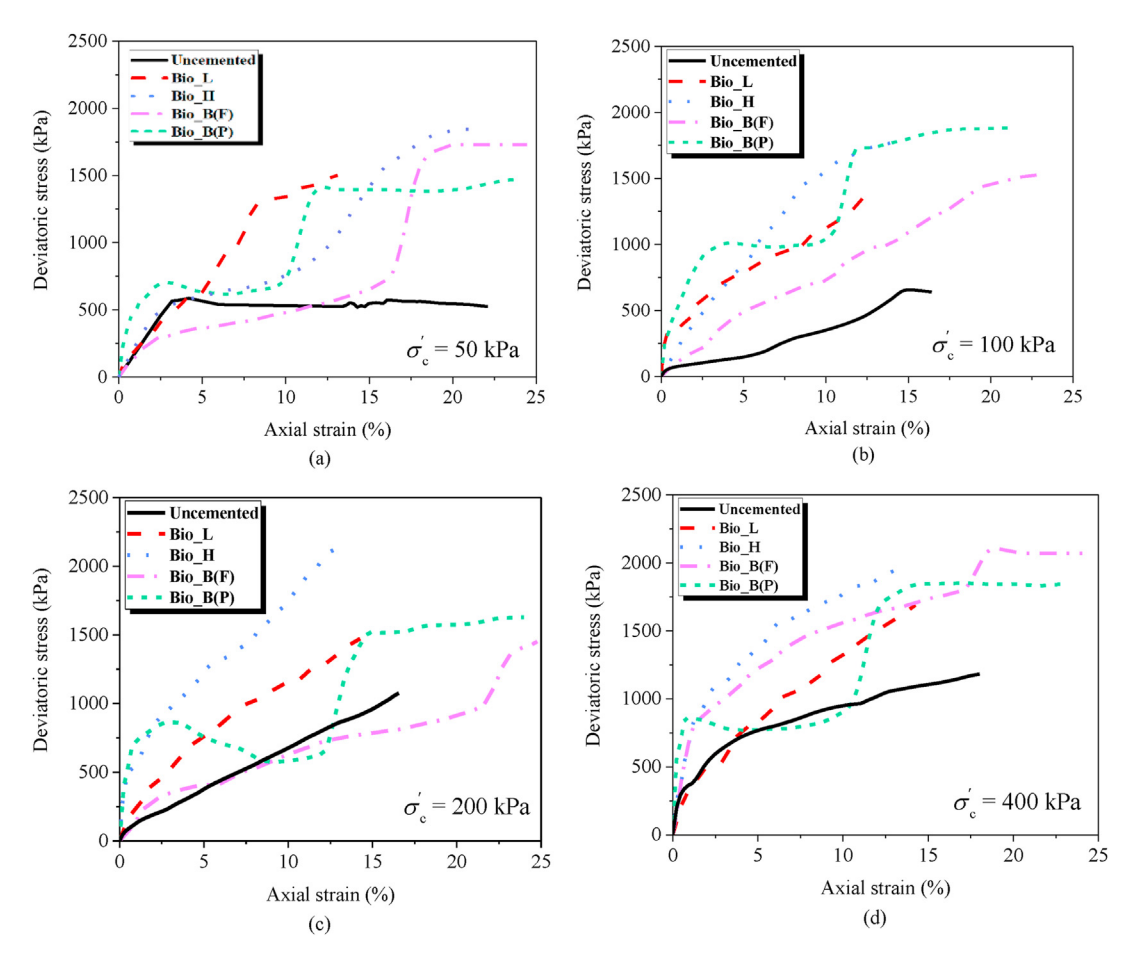


Fig. 6. The stress-strain behaviors of untreated and MICP-treated sand prepared at different confining pressure.

cementation of low liquid limit residual silt using Bacillus megaterium and cementation solutions with concentrations of 0.25 M, 0.5 M, and 1.0 M, maintaining an equal molar ratio of urea to calcium. The strength of the biocemented soil exhibited an increase of 26%-57% at 0.25 M, 25%-69% at 0.5 M, and no significant change at 1 M. respectively. This observation in the bioaugmentation process is consistent with the results in this study. From a microscopic perspective. Soon et al. (2014) also investigated the crystal morphology and distribution of calcite in samples treated with varying cementation solution concentrations using scanning electron microscopy (SEM). Their findings revealed that calcite primarily developed in the contact areas between soil particles, with the densest distribution occurring at a concentration of 0.5 M. In conclusion, employing a cementation solution concentration of 0.5 M in the biostimulated MICP process is deemed preferable. This finding aligns with previous research outcomes based on bioaugmentation. Hence, in subsequent experiments, a 0.5 M cementation solution concentration will be utilized, as determined by the optimization through unconfined compressive tests.

#### 3.2. Cementation content of biochar-assisted biocemented sand

The average CC and  $q_u$  values of biochar-assisted and nonbiochar-assisted biocemented sand prepared under different conditions are presented in Fig. 5. In the absence of biochar, the average CC increased as the duration of the cementation phase extends. Specifically, the average CC rises from 3.85% in Bio\_L to 5.63% in Bio\_H, which can be attributed to the addition of more cementation solution. For biochar-assisted biocemented sand, the CC of specimen Bio\_B(F), containing 0.3% flaked biochar, is 6.15%, marginally higher than that of Bio\_H. However, a notable increase in CC (8.42%) is observed in sample Bio\_B(P), which contains 0.3% powdered biochar. This can be attributed to the fact that powdered biochar. with its smaller size, can be distributed more evenly throughout the specimen compared to the larger-sized flaked biochar, thereby facilitating a greater increase in cementation content. It is worth noting that the Bio\_B(F) specimen, despite having a higher CC, demonstrated a lower  $q_u$  compared to Bio\_H as shown in Fig. 5. This observation suggests that the size of biochar plays a significant role in influencing the mechanical properties of the biocemented sand. Consequently, the  $q_{ij}$  appears to be a more suitable parameter for evaluating strength in comparison to CC, particularly when considering the influence of biochar particle size.

#### 3.3. Undrained shearing behaviors

Figs. 6 and 7 illustrate the changes in deviatoric stress ( $q = \sigma'_1$  –  $\sigma_3'$ ) and excess pore water pressure ( $\Delta u$ ) with respect to axial strain  $(\varepsilon_{\rm a})$  for uncemented, biocemented, and biochar-assisted biocemented specimens. These specimens were prepared under similar initial  $D_r$  and subjected to confining stresses ( $\sigma'_c$ ) of 50 kPa, 100 kPa, 200 kPa, and 400 kPa. As reference, uncemented specimens displayed a slight strain-softening behavior under  $\sigma_c' = 50$  kPa, while exhibiting strain-hardening behavior under higher  $\sigma'_{c}$ . For biocemented specimens, the majority displayed an initial linear elastic response when the axial strain was minimal (less than 2.5%), subsequently transitioning into a nonlinear strainhardening phase. The strain-hardening behavior can be attributed to the progressive mobilization of interparticle bonds, which conferred increasing resistance against deformation as the strain intensified. Interestingly, a strain-softening behavior followed by strain-hardening was observed in biocemented sand, particularly in the Bio\_B(P) at  $\sigma_{\rm c}'=50$  kPa, 100 kPa, 200 kPa, and 400 kPa. The axial strain during the transition from strain-softening to strainhardening behavior was observed to range between 7% and 10%. A combination of interrelated factors could potentially contribute to this phenomenon:

- (1) Heterogeneity of cementation. The distribution of cementation within the soil sample may not be homogeneous, resulting in regions with varying bond strengths. As the test progresses, weaker bonds are likely to break first, displaying strain-softening behavior. Conversely, stronger bonds in other regions may remain intact. As the load is further applied, these stronger bonds contribute to the observed strain-hardening behavior.
- (2) Particle rearrangement and interlocking. As the weaker cementation breaks, sand particles undergo rearrangement and interlocking, creating a denser packing configuration. Additionally, the breaking of interparticle bonds during the strain-softening phase results in stress redistribution among the remaining bonds and sand particles. As the axial strain reaches 7%—10%, the stresses are redistributed in a way that the remaining cementation bonds and inter-particle contacts can effectively resist further deformation, leading to strainhardening behavior.

The  $\Delta u$  response initially displayed a positive value, which is indicative of a contractive tendency. Subsequently, it transitioned to a negative value, signifying a pronounced propensity of dilation for all specimens. In addition, the  $\Delta u$  clearly showed a dependence on the  $\sigma_c'$  and  $q_u$ , with a higher  $\Delta u$  (positive) observed in specimens subjected to greater  $\sigma_c'$  and  $q_u$ . Conversely, at smaller  $\sigma_c'$  and  $q_u$ , the specimens tended to experience negative  $\Delta u$  at low strains. Nevertheless, in this study, none of the specimens exhibited an overall positive  $\Delta u$  at a maximum  $\sigma_c' = 400$  kPa. The biocemented sand demonstrated dilative behavior, which can potentially be attributed to the brittle nature of cementation between particle contacts. This characteristic may induce localized dilation within the shear band under loading conditions.

Fig. 8 displays the post-failure features of specimens subjected to shearing at  $\sigma_c' = 200$  kP. The uncemented specimen and Bio\_L with lower  $q_u$  both exhibited bulging-type failures. However, the extent of bulging varied slightly, with the Bio\_L demonstrating less bulging compared to the uncemented specimen. As  $q_u$  increased, a distinct shear band appeared in Bio\_H, spanning the entire length of the specimen. In the case of biochar-assisted biocemented specimens (i.e. Bio\_B(F) and Bio\_B(P)), multiple shear bands were generated, and the thickness of these bands became more pronounced and substantially wider. It was observed that Bio\_B(F) exhibited the highest number of shear bands among all specimens, indicative of a considerably inhomogeneous distribution of biocementation.

#### 3.4. Failure criterion and effective stress path

Most previous studies investigating the behavior of cemented soils have primarily focused on drained triaxial tests, leaving the undrained behavior relatively underexplored. Characterizing the strength of cemented soils under undrained loading conditions poses a significant challenge, as there is often a lack of agreement between the strengths obtained from drained and undrained tests (Haeri et al., 2005; Baxter et al., 2011). The limited studies on undrained behavior have yielded inconsistent results, further highlighting the complexity of understanding the strength of cemented soils under undrained loading conditions.

Considering the stress-strain behaviors illustrated in Fig. 6, the peak deviatoric stress proves to be an inadequate failure criterion

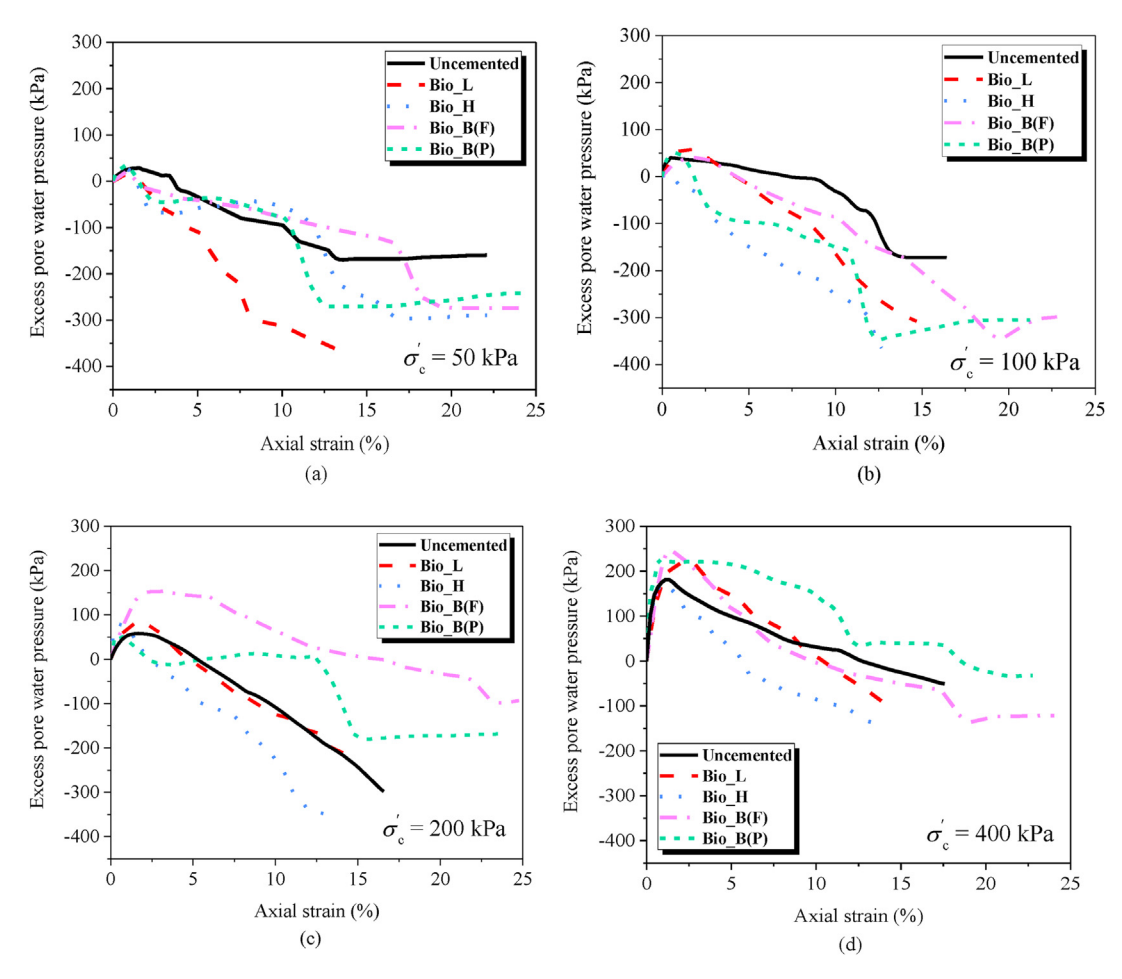


Fig. 7. The excess pore water pressure behaviors of untreated and MICP-treated sand prepared at different confining pressure.

for biocemented sand, although it is the most widely used criterion for many different types of tests and soils. Consequently, selection of an appropriate failure criterion to accurately determine the shearing parameters becomes of paramount importance for the analysis and design of geotechnical structures involving biocemented sand. In the present study, two distinct failure criteria were employed: maximum principal stress ratio  $((\sigma'_1 - \sigma'_3)_{\text{max}})$ , and Skempton's pore pressure parameter  $\overline{A} = 0$ . Utilizing  $\overline{A} = 0$  as a failure criterion effectively eliminates variability between undrained tests and ensures that the mobilized failure strength is not reliant on the highly variable negative excess pore pressures

(Baxter et al., 2011). This criterion has been applied in previous studies focusing on weakly cemented soils (Amini and Hamidi, 2014; Karimian and Hassanlourad, 2022), further supporting its applicability in characterizing the failure of such materials. Baxter et al. (2011) indicated that an increase in CC amplifies the discrepancies between cohesion intercept values calculated under drained and undrained conditions using the  $\overline{A} = 0$  failure criterion. However, the type of cementation involved in their study and the current research differs. The calcium carbonate formed after the MICP treatment is considerably weaker than the ordinary Portland cement (OPC) employed in their study. Despite the maximum CC of

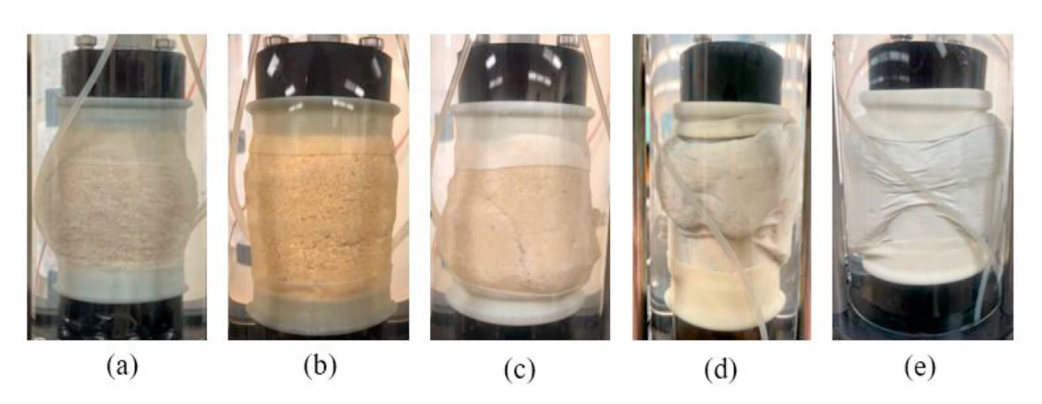


Fig. 8. The post-failure characteristics of specimens under  $\sigma_c' = 200$  kPa: (a) Uncemented, (b) Bio\_L, (c) Bio\_H, (d) Bio\_B(F), and (e) Bio\_B(P).

biocementation exceeding 8% in the present study, which is significantly higher than the 2.5%CC of OPC in their study, the utilization of unconfined compressive strength ( $q_{\rm u}$ ) becomes more rational. As per Baxter et al. (2011), the application of the  $\overline{A}=0$  failure criterion is considered appropriate when the unconfined compressive strength  $q_{\rm u}<1807$  kPa. In the current study, the average  $q_{\rm u}$  values for all specimens, as outlined in Table 4, are found to be below the threshold of 1807 kPa, supporting the suitability of employing the  $\overline{A}=0$  failure criterion for this dataset.

Fig. 9 displays the failure points on the effective stress path plots

and under failure criteria of  $((\sigma'_1 - \sigma'_3)_{max})$  and  $\overline{A} = 0$ , respectively. For both uncemented specimens and biocemented specimens subjected to higher confining pressures (i.e. 200 kPa and 400 kPa), the effective stress path initially moved towards the left, signifying a contractive tendency accompanied by positive  $\Delta u$ . For specimens amended with powdered biochar (i.e. Bio\_B(P)), as evidenced by the stress-strain curves in Fig. 6, the effective stress path exhibits a reversal in direction during shearing, indicating a transition from strain-softening to strain-hardening behavior. Fig. 10 presents a representative effective stress for various specimens subjected to

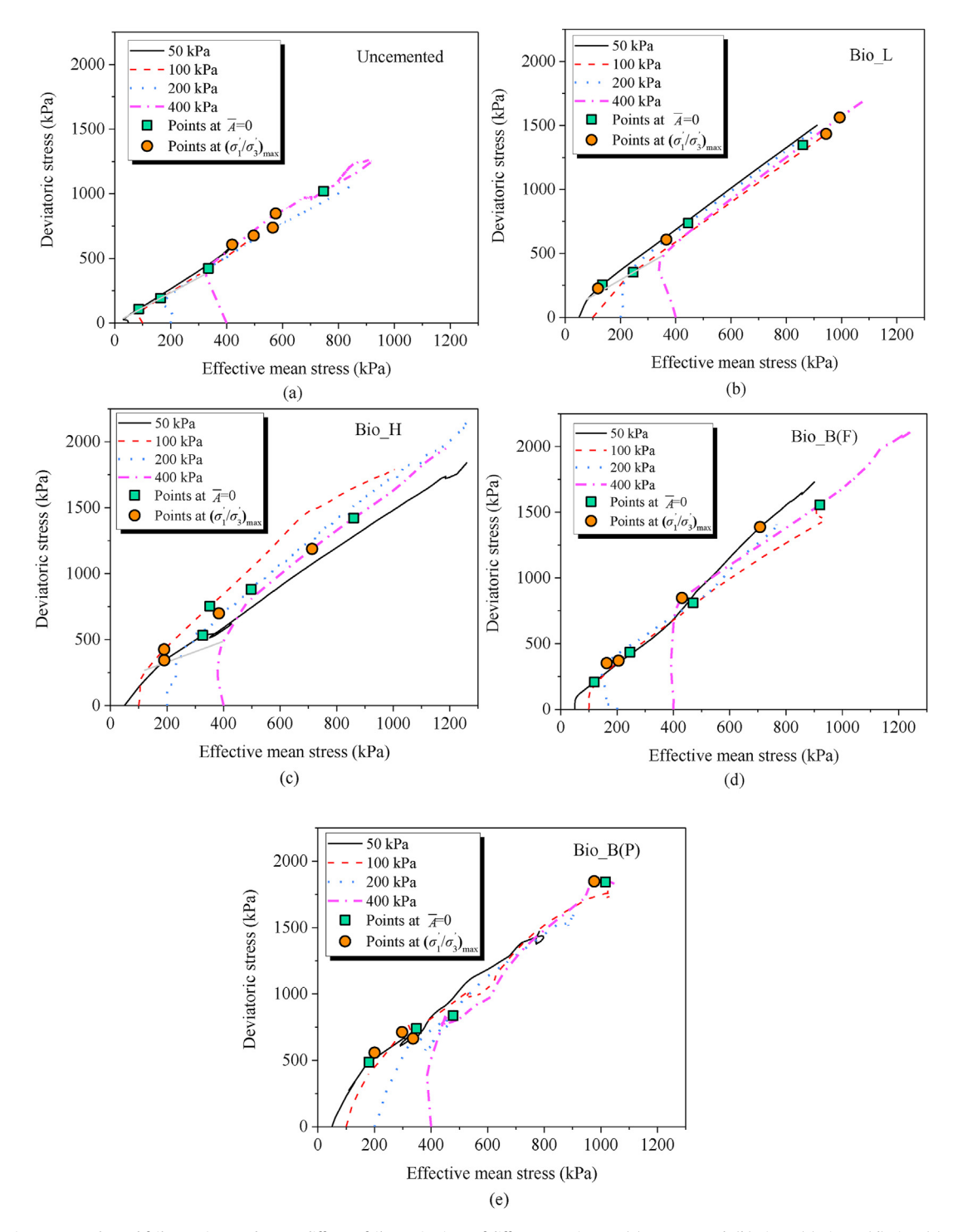


Fig. 9. The effective stress paths and failure points under two different failure criterions of different specimens: (a) uncemented; (b) Bio\_L; (c) Bio\_H; (d) Bio\_B(F); and (e) Bio\_B(P).

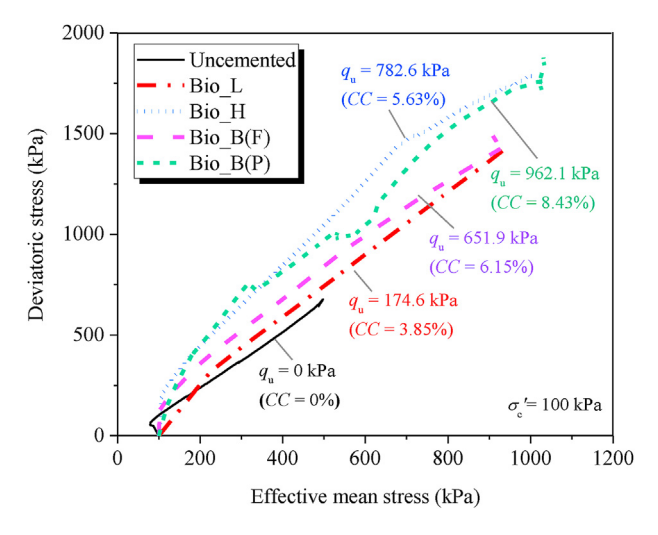


Fig. 10. The effective stress paths under 100 kPa confining pressure.

confining pressure  $\sigma_c'=100$  kPa. As  $q_u$  increases, a higher deviatoric stress was observed during shearing, causing the effective stress path to shift upward. Under  $\sigma_c'=100$  kPa, Bio\_H and Bio\_B(P) exhibited similar variations in tendency with the comparably highest deviator stress, followed by Bio\_B(F), Bio\_L, and the uncemented specimen.

#### 3.5. Failure envelopes and shearing parameters

The effective stress strength parameters, cohesion (c') and friction angle  $(\varphi')$ , derived from the Mohr-Coulomb theory, are extensively employed in geotechnical practice to quantify soil strength. The failure envelopes for the cemented sand are not always linear, which becomes a challenge in the accurate characterization of their mechanical behavior using traditional linear failure envelope (Sharma et al., 2011; Nafisi et al., 2020). It has been demonstrated that a linear envelope may lead to overestimation of the shear strength, particularly the cohesion intercept, at low confinements if the failure envelope is fitted to data derived from relatively high confinements (Jiang et al., 2003). Furthermore, in the undrained triaxial test, due to the experimental conditions that do not allow water molecules to be expelled from the sample, the changes in pore water pressure can affect the strength performance of the sample. Therefore, the nonlinear failure envelopes may be better to describe the material behavior. The nonlinearity of failure envelopes for cemented sand can be attributed to the intricate interactions, breakage of interparticle bonds and rearrangements of sand particles under loading conditions, as well as changes in stress paths and mobilization of interparticle forces. In the present study, a generalized form of the strength function is employed to define the nonlinear Mohr envelope for biocemented sands (Baker, 2004; Sharma et al., 2011). This strength function is expressed as follows:

$$\tau = P_{a}A \left(\frac{\sigma'}{P_{a}} + T\right)^{n} \tag{3}$$

where  $\tau$  is the shear strength;  $\sigma'$  is the normal stress; A, T, and n are the nondimensional constants; and  $P_a$  is the atmospheric pressure. The parameter A serves as a scaling factor that governs the magnitude of shear strength. The parameter T functions as an allocation factor, determining the intercept of the envelope. Meanwhile, the parameter T dictates the curvature of the envelope, providing flexibility in capturing the nonlinear behavior of

biocemented sands. The following three requirements should be satisfied to meet the basic logical conditions for Mohr failure envelope: A>0,  $0.5\leq n\leq 1$ , and  $T\geq 0$ . To fit the data set of stress points  $(\sigma'_{1\mathrm{f}}$  and  $\sigma'_{3\mathrm{f}})$  based on specific failure criterion with nonlinear Mohr failure envelope, the normal  $(\sigma'_{\mathrm{ff}})$  and shear stress  $(\tau_{\mathrm{ff}})$  on the failure plane can be written as

$$\sigma'_{ff} = \frac{\sigma'_{1f} + \sigma'_{3f}}{2} - \frac{\sigma'_{1f} - \sigma'_{3f}}{2} \sin(\varphi')$$
 (4)

$$\tau_{\rm ff} = \frac{\sigma_{\rm 1f}' - \sigma_{\rm 3f}'}{2} \cos(\varphi') \tag{5}$$

The tangential friction angle  $\varphi'$  at any  $\sigma'$  can be calculated by

$$\tan \varphi'|_{\sigma'} = \frac{\mathrm{d}\tau}{\mathrm{d}\sigma} = \frac{An}{\left(\frac{\sigma'}{P_{\mathrm{a}}} + T\right)^{1-n}} \tag{6}$$

To plot the nonlinear failure envelops, the four pairs of values of  $\sigma'_{\rm ff}$  and  $\tau_{\rm ff}$  were first calculated using the obtained triaxial test data and Eqs. (4) and (5), under the assumption that the initial friction angle  $\varphi'=0$ . The first set of parameters  $\{A,T,n\}$  was then derived through nonlinear least square curve fitting, implemented in Matlab, and verified to ensure they were within the abovementioned specified range. The new  $\varphi'$  was subsequently computed using Eq. (6) and the obtained parameters  $\{A,T,n\}$  during the first iteration. This iteration process continued until the difference between the calculated  $\varphi'$  values in two consecutive iterations was less than  $0.0001^\circ$ .

Fig. 11 compares the linear and nonlinear failure envelopes under  $(\sigma'_1 - \sigma'_3)_{\text{max}}$  and  $\overline{A} = 0$  failure criterions for all specimens. The obtained parameters  $\{A, T, n\}$  and c' are listed in Tables 5–8. Regardless of the failure criterion and envelope applied, it was evident that the c' value increased with the rise in CC for biocemented specimens without biochar amendment. For the biocharassisted specimens, the value of c' for Bio\_B(F) was close to zero, even lower than that of Bio\_L, despite the higher CC induced compared to Bio\_L and Bio\_H. This finding implies that flaked biochar may not significantly contribute to interparticle bonding at low confinement conditions. Furthermore, when comparing the linear and nonlinear failure envelopes based on the  $(\sigma'_1 - \sigma'_3)_{max}$ failure criterion, a lower confining pressure (5-11 kPa) and a smaller c' value were observed for the non-biochar-assisted specimens (i.e. Bio\_L and Bio\_H) using the nonlinear failure envelope. In contrast, no significant difference (<2 kPa) was found between linear and nonlinear failure envelopes in the biochar-assisted specimens (i.e. Bio\_B(F) and Bio\_B(P)). Moreover, employing the  $\overline{A} = 0$  failure criterion resulted in a more conservative estimation compared to using the  $(\sigma'_1 - \sigma'_3)_{max}$  failure criterion, as a smaller value of c' was obtained, particularly in the context of a nonlinear failure envelope. However, this conservative estimation of c' was not as pronounced when considering a linear failure envelope, which might be attributed to the scattered data within the relatively low confinement range. Lastly, it was observed that the  $\overline{A} = 0$ failure criterion (dashed lines in Fig. 11) predicts a significantly lower shear stress compared to the  $(\sigma'_1 - \sigma'_3)_{max}$  failure criterion (solid lines in Fig. 11), particularly across a broader range of normal stress. It is worth noting that the accuracy of shear strength between different failure criteria has not been addressed in this discussion.

Fig. 12 shows the normalized value of c' by the CC under various failure criteria (denoted as c'/CC). The c'/CC can be used to compare the efficiency of cohesion increase per unit of cementation content

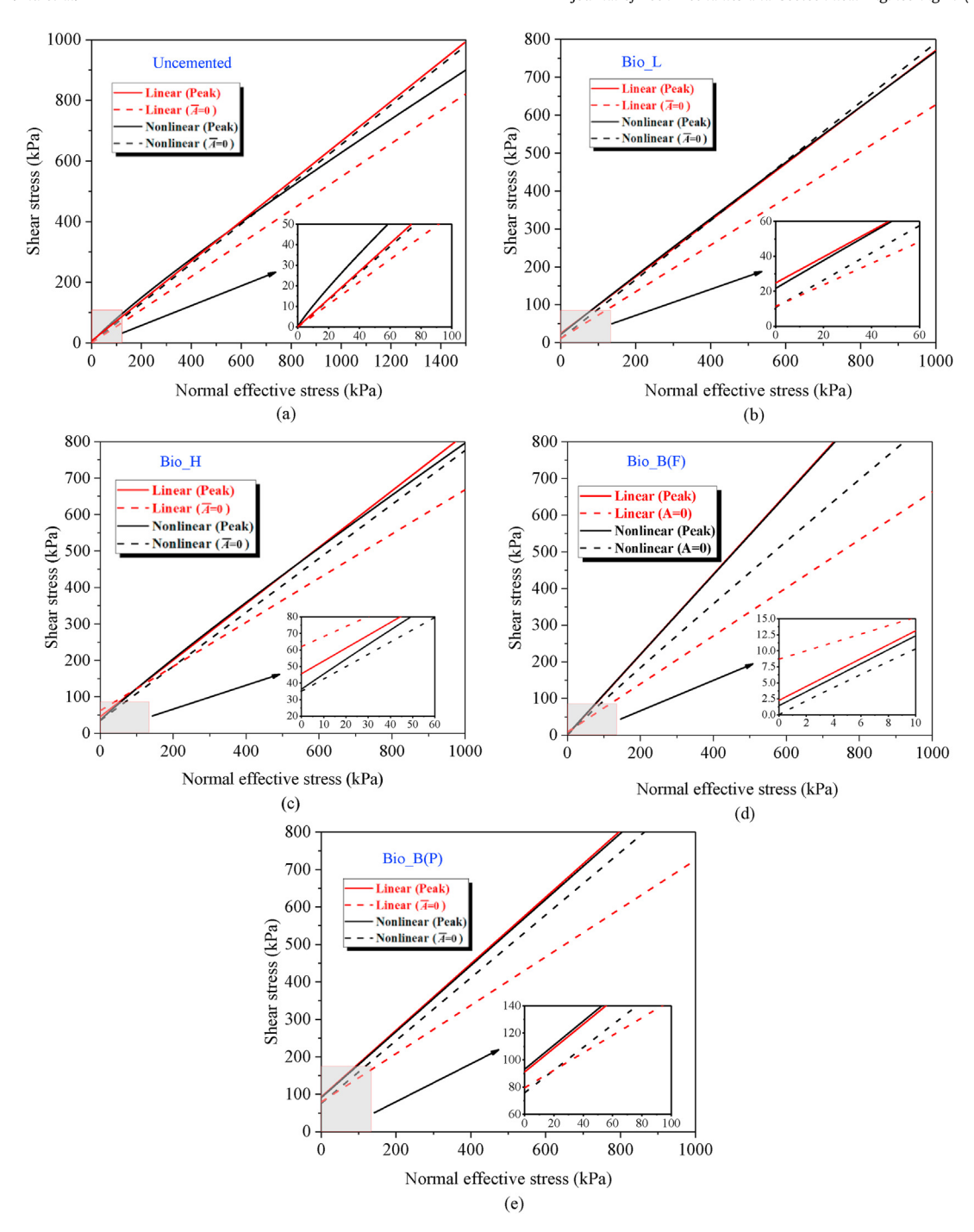


Fig. 11. The comparison between linear and non-linear failure envelopes under two different failure criterions for different specimens: (a) uncemented; (b) Bio\_L; (c) Bio\_H; (d) Bio\_B(F); and (e) Bio\_B(P).

**Table 5** The shear strength parameters calculated from nonlinear failure envelopes based on the  $(\sigma'_1-\sigma'_3)_{\max}$  failure criterion.

Specimen	Α	T	n	c' (kPa)
Untreated	0.805	0.000	0.891	0
Bio_L	0.800	0.260	0.972	21.89
Bio_H	0.925	0.362	0.921	36.76
Bio_B(F)	1.088	0.021	1.000	1.43
Bio_B(P)	0.882	1.033	1.000	92.32

**Table 6** The shear strength parameters calculated from nonlinear failure envelopes based on the  $\overline{A}=0$  failure criterion.

Specin	nen	Α	T	п	<i>c</i> ′ (kPa)
Untrea	ited	0.654	0.000	1.000	0.00
Bio_L		0.779	0.139	1.000	10.97
Bio_H		0.745	0.470	0.998	35.02
Bio_B(	F)	0.944	0.000	0.962	0.00
Bio_B(	P)	0.838	0.904	1.000	76.80

**Table 7** The shear strength parameters calculated from linear Mohr-Coulomb failure envelopes based on the  $(\sigma'_1 - \sigma'_3)_{\max}$  failure criterion.

Specimen	φ (°)	c' (kPa)
Untreated	34.41	0
Bio_L	36.72	26.68
Bio_H	37.76	47.97
Bio_B(F)	47.53	1.25
Bio_B(P)	41.62	90.35

**Table 8** The shear strength parameters calculated from linear Mohr-Coulomb failure envelopes based on the  $\overline{A}=0$  failure criterion.

Specimen	$\varphi$ (°)	c' (kPa)
Untreated	33.21	0
Bio_L	38.02	11.39
Bio_H	37.30	62.06
Bio_B(F)	40.92	8.69
Bio_B(P)	40.21	79.49

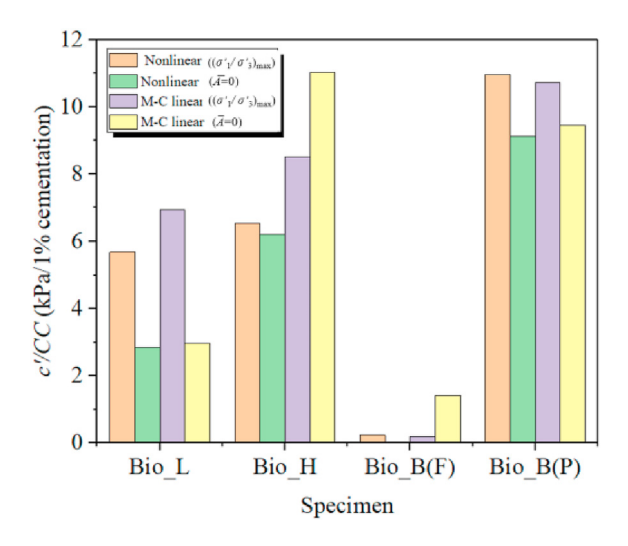


**Fig. 12.** The normalized effective cohesion by cementation content under various failure criteria.

across different specimens. It allows for a direct comparison of the bonding strength relative to the amount of  $CaCO_3$ , irrespective of the absolute quantities. Irrespective of the selected failure criteria and the nature of the failure envelope employed, the  $Bio_B(P)$  and  $Bio_B(P)$  and  $Bio_B(P)$  demonstrated a relatively greater increase in c' per unit of CC compared to their counterparts, followed by  $Bio_B(D)$ . Conversely, the specimen  $Bio_B(P)$  manifested the least value of c' / CC suggesting that the incorporation of flaked biochar of a larger size may exert a negative influence on the enhancement of cohesion. Although the absolute value of CC in  $Bio_B(F)$  experienced an upward trend in comparison to the control specimen devoid of biochar amendment, the efficiency of increase was markedly diminished.

#### 3.6. Microscopic characteristics

The observed enhancement in shear strength and cohesion of biochar-assisted biocemented sand can be attributed to the development of interparticle bonds and alterations in particle roughness, as evidenced by the microscopic features presented in Fig. 13. In comparison to the biocemented specimen Bio\_H without biochar amendment (Fig. 11b), the biocementation in Bio\_B(P) is

much darker with biochar powder embedded within the biocementation. This suggests that the powdered biochar can effectively serve as additional nucleation sites, thereby increasing the CC. Concurrently, it was observed that flaked biochar, with its larger size, can also provide extra nucleation sites during the MICP process, as evidenced by a noticeable layer of white biocementation adhering to the biochar flake's surface. However, most of this biocementation did not function as effective interparticle bridges within the soil matrix. As a result, despite the increase in CC for Bio\_B(F), its shear strength and cohesion did not exhibit significant enhancement compared to Bio\_B(P). Furthermore, a larger biochar size contributed to a more inhomogeneous distribution of biocementation. These combined mechanisms ultimately led to low absolute value of c' and c'/CC for Bio\_B(F), regardless of the applied failure criterion.

#### 3.7. Discussion

Based on the results, it is evident that biochar positively influences the increase in CC and the enhancement of shearing strength parameters under CU triaxial testing. To gain a deeper understanding of the role of biochar during biostimulated MICP process, a series of solution batch tests were conducted to investigate the effect of biochar on the ureolytic activity. In the batch test, triplicate samples were prepared to ensure the accuracy and reliability of the results. The investigation only involved the enrichment phase by mixing the collected calcareous sand with enrichment media. The detailed procedures are outlined in the 2.2 section. Fig. 14 displays the variation in ureolytic activity of the bacterial solution within 108 h after inclusion of the biochar. Generally, a significant increase in UA was observed at the 24-h mark for all cases, with the UA eventually reaching its peak value before declining. Notably, biochar-assisted solutions demonstrated higher UA compared to non-biochar-assisted solutions throughout the entire enrichment process. Solutions amended with a greater amount of biochar (i.e. 4 g) exhibited higher UA compared to those containing a lesser amount of biochar (i.e. 2 g). Moreover, this study also considered the sterilization conditions. It was observed that,

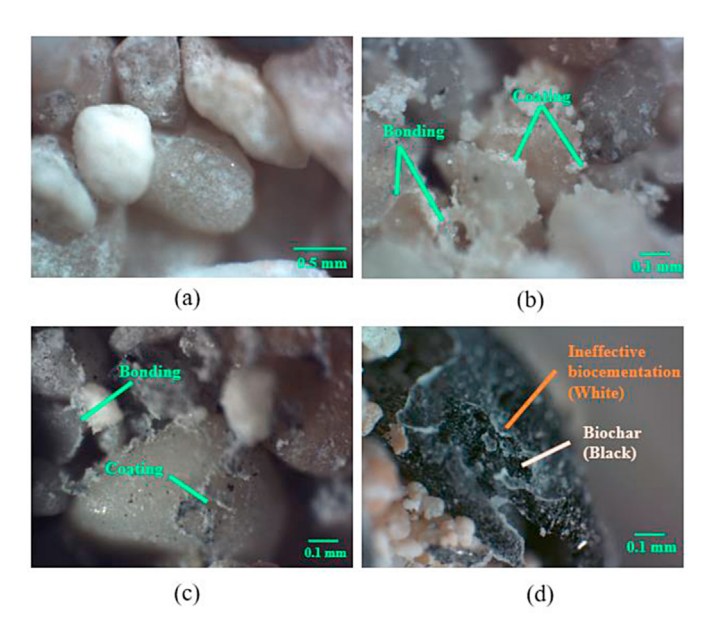


**Fig. 13.** The microscopic features of test specimen: (a) Uncemented specimen, (b) the characteristics of bonding and coating in Bio\_H, (c) the characteristics of bonding and coating in Bio\_B(P), and (d) the ineffective biocementation in Bio\_B(F).

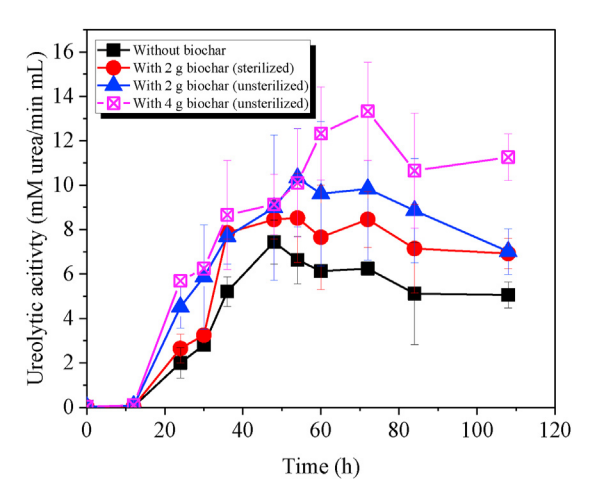


Fig. 14. The Effect of biochar on ureolytic activity over time.

for a given biochar content (e.g. 2 g), the unsterilized condition led to higher ureolytic activity compared to the sterilized condition. This suggests that the unsterilized condition promotes the growth of indigenous ureolytic bacteria more effectively, which is favorable for the potential field application. As indicated in previous research, biochar has been shown to markedly promote bacterial growth through various mechanisms. Verheijen et al. (2010) highlights that biochar typically possesses a high cation exchange capacity. Biochar's high cation exchange capacity can help maintain an optimal ionic environment for ureolytic bacteria in the solution, promoting their growth and urease activity. Additionally, biochar can help buffer the pH of the solution, maintaining optimal pH conditions for the growth and enzymatic activity of ureolytic bacteria. It should be noted that the pH value of biochar was around 9.1  $\pm$  0.2. Urease activity is generally pH-dependent, and an optimal pH range (approximately 9.0) can enhance the enzyme's activity (Wang et al., 2020). Finally, biochar can adsorb potentially toxic compounds, such as heavy metals, pesticides, and organic pollutants in the bacterial solution (Beesley et al., 2010), which can reduce their toxicity and create a less stressful environment for bacterial growth. In transitioning from a solution-based environment to soil, biochar can enhance nutrient availability for bacteria through the adsorption and retention of essential nutrients, such as nitrogen and phosphorus, within its structure. This improved nutrient accessibility can foster bacterial growth and activity. Moreover, the micropores within biochar also serve as refuges for microorganisms, leading to increased microbial biomass in soil, as reported by Kolb et al. (2009). Given the aforementioned roles of biochar in soil, it is reasonable to hypothesize that MICP, a process heavily dependent on soil-microbe interactions, can be enhanced through addition of the biochar. It is important to note, however, that the effectiveness of biochar in promoting enzymatic activity may vary depending on the type of biochar. Further investigation into the influence of different biochar types on ureolytic activity is required.

#### 4. Conclusions

In this study, the viability of biochar-assisted biostimulated MICP for enhancing the shear strength of calcareous sand is explored. The optimal cementation solution for biostimulated MICP is initially determined through a series of unconfined compressive tests. The shear properties of biocemented calcareous sand, augmented by biochar and treated via biostimulation, are assessed using CU triaxial shear tests. To characterize the shear strength of biocemented sand under low effective normal stress, both Mohr-Coulomb failure envelopes and nonlinear failure envelopes are

utilized. Moreover, the study compares and analyzes two distinct stress states to identify a suitable failure criterion. Additionally, the microscopic features and post-failure characteristics of biocharassisted biocemented calcareous sand are examined. Based on the analysis and discussion of the results, the following conclusions can be drawn:

- (1) Utilizing a moderate cementation solution concentration of 0.5 M in the biostimulated MICP process is considered more favorable compared to concentrations of 0.1 M and 1 M. An extended duration of the cementation stage can yield higher  $q_{\rm u}$  and  $E_{50}$  in the context of unconfined compressive tests within a 10-d cementation treatment period.
- (2) The incorporation of biochar contributes to an increase in *CC*. Non-biochar-assisted specimens with lower  $q_{\rm u}$  exhibit strain-hardening behaviors, whereas biochar-assisted specimens with higher  $q_{\rm u}$  demonstrate a transition from strain-softening to strain-hardening behavior within the range of 7%–10% strain. Employing the  $\overline{A}=0$  failure criterion results in a more conservative estimation in shear stress value and c' compared to the  $(\sigma'_1-\sigma'_3)_{\rm max}$  failure criterion.
- (3) Based on the post-failure characteristics of all specimens, multiple shear bands are generated in the biochar-assisted samples, indicating a significantly inhomogeneous distribution of biocementation. The thickness of these bands becomes more distinct and considerably wider. Moreover, according to the microscopic images, powdered and flaked biochar can both serve as additional nucleation sites for cementation, however the increase of cementation by flaked biochar shows less efficient on improving the shear strength.
- (4) Biochar can increase the UA during biostimulated MICP process in the context of solution test. Solutions containing a larger amount of biochar (i.e. 4 g) demonstrated a higher UA value compared to those with a smaller quantity of biochar (i.e. 2 g). Additionally, the unsterilized condition more effectively promotes the growth of indigenous ureolytic bacteria.

#### CRediT authorship contribution statement

Yijie Wang: Writing — original draft, Methodology, Conceptualization. Xiaole Han: Writing — review & editing, Validation. Kaiwei Liu: Writing — review & editing. Juan Du: Writing — review & editing. Wenbo Chen: Writing — review & editing, Funding acquisition. Zhenyu Yin: Writing — review & editing, Supervision, Funding acquisition. Shu Yu: Writing — review & editing. Ningjun Jiang: Writing — review & editing, Supervision, Methodology, Investigation, Funding acquisition, Conceptualization.

#### Declaration of generative Al and Al-assisted technologies in the writing process

During the preparation of this work the authors used the ChatGPT in order to improve readability and language. After using this tool/service, the authors reviewed and edited the content as needed and take full responsibility for the content of the publication.

#### **Declaration of competing interest**

The authors declare that they have no known competing financial interests or personal relationships that could have appeared to influence the work reported in this paper.

#### **Acknowledgments**

This study is financially supported by the Natural Science Foundation of China (Grant Nos. 42377166 and 42007246), Key R&D Program Social Development Project of Jiangsu Province (Grant No. BE2023800), and the National Key R&D Program of China (Grant No. 2023YFC3709600).

#### References

- Amini, Y., Hamidi, A., 2014. Triaxial shear behavior of a cement-treated sand—gravel mixture. J. Rock Mech. Geotech. Eng. 6 (5), 455–465.
- Baker, R., 2004. Nonlinear Mohr envelopes based on triaxial data. J. Geotech. Geoenviron. 130 (5), 498–506.
- Baxter, C.D., Ravi Sharma, M.S., Moran, K., Vaziri, H., Narayanasamy, R., 2011. Use of A= 0 as a failure criterion for weakly cemented soils. J. Geotech. Geoenviron. 137 (2), 161–170.
- Beesley, L., Moreno-Jiménez, E., Gomez-Eyles, J.L., 2010. Effects of biochar and greenwaste compost amendments on mobility, bioavailability and toxicity of inorganic and organic contaminants in a multi-element polluted soil. Environ. Pollut. 158 (6), 2282–2287.
- Brandes, H.G., 2011. Simple shear behavior of calcareous and quartz sands. Geotech. Geol. Eng. 29, 113–126.
- Burdalski, R.J., Gomez, M.G., 2020. Investigating the effect of microbial activity and chemical concentrations on the mineralogy and morphology of ureolytic biocementation. In: Geo-Congress 2020: Biogeotechnics. American Society of Civil Engineers, Reston, VA, pp. 83–95.
- Chan, K.Y., Van Zwieten, L., Meszaros, I., Downie, A., Joseph, S., 2007. Agronomic values of greeniste biochar as a soil amendment. Soil Res. 45 (8), 629–634.
- Gat, D., Ronen, Z., Tsesarsky, M., 2016. Soil bacteria population dynamics following stimulation for ureolytic microbial-induced CaCO3 precipitation. Environ. Sci. Technol. 50 (2), 616–624.
- Gomez, M.G., Anderson, C.M., Graddy, C.M., DeJong, J.T., Nelson, D.C., Ginn, T.R., 2015. Stiffness and strength of bio-cemented calcareous sand. J. Geotech. Geoenviron. 141 (12), 04015054.
- Gomez, M.G., Anderson, C.M., Graddy, C.M., DeJong, J.T., Nelson, D.C., Ginn, T.R., 2017. Large-scale comparison of bioaugmentation and biostimulation approaches for biocementation of sands. J. Geotech. Geoenviron. 143 (5), 04016124.
- Gowthaman, S., Mitsuyama, S., Nakashima, K., Komatsu, M., Kawasaki, S., 2019. Biogeotechnical approach for slope soil stabilization using locally isolated bacteria and inexpensive low-grade chemicals: a feasibility study on Hokkaido expressway soil, Japan. Soils Found. 59 (2), 484–499.
- Haeri, S.M., Hosseini, S.M., Toll, D.G., Yasrebi, S.S., 2005. The behaviour of an artificially cemented sandy gravel. Geotech. Geol. Eng. 23, 537–560.
- Jiang, J.C., Baker, R., Yamagami, T., 2003. The effect of strength envelope nonlinearity on slope stability computations. Can. Geotech. J. 40 (2), 308–325.
- Jiang, N.J., Liu, R., Du, Y.J., Bi, Y.Z., 2019. Microbial induced carbonate precipitation for immobilizing Pb contaminants: toxic effects on bacterial activity and immobilization efficiency. Sci. Total Environ. 672, 722–731.
   Jiang, N.J., Wang, Y.J., Chu, J., Kaisaki, S., Tang, C.S., Cheng, L., Du, Y.J., Shashank, B.S.,
- Jiang, N.J., Wang, Y.J., Chu, J., Kaisaki, S., Tang, C.S., Cheng, L., Du, Y.J., Shashank, B.S., Singh, D.N., Han, X.L., Wang, Y.Z., 2022. Bio-mediated soil improvement: an introspection into processes, materials, characterization and applications. Soil Use Manag. 38 (1), 68–93.
- Karimian, A., Hassanlourad, M., 2022. Mechanical behaviour of MICP-treated silty sand. Bull. Eng. Geol. Environ. 81, 285. https://doi.org/10.1007/s10064-022-02780-2.
- Khan, M.N.H., Ggnn, A., Shimazaki, S., Kawasaki, S., 2015. Coral sand solidification test based on microbially induced carbonate precipitation using ureolytic bacteria. Mater. Trans. 56 (10), 1725–1732.
- Knorst, M.T., Neubert, R., Wohlrab, W., 1997. Analytical methods for measuring urea in pharmaceutical formulations. J. Pharm. Biomed. Anal. 15 (11), 1627–1632.
- Kolb, S.E., Fermanich, K.J., Dornbush, M.E., 2009. Effect of charcoal quantity on microbial biomass and activity in temperate soils. Soil Sci. Soc. Am. J. 73 (4), 1173–1181.
- Lai, Y., Yu, J., Liu, S., Liu, J., Wang, R., Dong, B., 2021a. Experimental study to improve the mechanical properties of iron tailings sand by using MICP at low pH. Construct. Build. Mater. 273, 121729.
- Lai, H.J., Cui, M.J., Wu, S.F., Yang, Y., Chu, J., 2021b. Retarding effect of concentration of cementation solution on biocementation of soil. Acta Geotech 16, 1457–1472.

- Liu, L., Liu, H., Xiao, Y., Chu, J., Xiao, P., Wang, Y., 2018. Biocementation of calcareous sand using soluble calcium derived from calcareous sand. Bull. Eng. Geol. Environ. 77, 1781–1791.
- Liu, L., Liu, H., Stuedlein, A.W., Evans, T.M., Xiao, Y., 2019. Strength, stiffness, and microstructure characteristics of biocemented calcareous sand. Can. Geotech. J. 56 (10), 1502—1513.
- Maksimovic, M., 1989. Nonlinear failure envelope for soils. J. Geotech. Eng. 115 (4), 581–586.
- Montoya, B.M., DeJong, J.T., 2015. Stress-strain behavior of sands cemented by microbially induced calcite precipitation. J. Geotech. Geoenviron. 141 (6), 04015019.
- Mujah, D., Cheng, L., Shahin, M.A., 2019. Microstructural and geomechanical study on biocemented sand for optimization of MICP process. J. Mater. Civ. Eng. 31 (4), 04019025
- Mwandira, W., Nakashima, K., Kawasaki, S., 2017. Bioremediation of lead-contaminated mine waste by Pararhodobacter sp. based on the microbially induced calcium carbonate precipitation technique and its effects on strength of coarse and fine grained sand. Ecol. Eng. 109, 57–64.
- Nafisi, A., Montoya, B.M., Evans, T.M., 2020. Shear strength envelopes of biocemented sands with varying particle size and cementation level. J. Geotech. Geoenviron. 146 (3), 04020002.
- Pakbaz, M.S., Ghezelbash, G.R., Afzal, A., 2020. Sugarcane molasses: a cheap carbon source for calcite production in different class of soils using stimulation of indigenous urease-producing bacteria. Geomicrobiol. J. 37 (3), 213–229.
- Sharma, M.R., Baxter, C.D., Hoffmann, W., Moran, K., Vaziri, H., 2011. Characterization of weakly cemented sands using nonlinear failure envelopes. Int. J. Rock Mech. Min. Sci. 48 (1), 146–151.
- Soon, N.W., Lee, L.M., Khun, T.C., Ling, H.S., 2014. Factors affecting improvement in engineering properties of residual soil through microbial-induced calcite precipitation. J. Geotech. Geoenviron. 140 (5), 04014006.
- Tang, C.S., Yin, L.Y., Jiang, N.J., Zhu, C., Zeng, H., Li, H., Shi, B., 2020. Factors affecting the performance of microbial-induced carbonate precipitation (MICP) treated soil: a review. Environ. Earth Sci. 79, 1–23.
- Vekariya, M.S., Pitroda, J., 2013. Bacterial concrete: new era for construction industry. Int. J. Eng. Trends Technol. 4 (9), 4128–4137.
- Verheijen, F., Jeffery, S., Bastos, A.C., Van der Velde, M., Diafas, I., 2010. Biochar application to soils. A critical scientific review of effects on soil properties, processes, and functions. EUR 24099, 162.
- Wang, Y.J., Han, X.L., Jiang, N.J., Wang, J., Feng, J., 2020. The effect of enrichment media on the stimulation of native ureolytic bacteria in calcareous sand. Int. J. Environ. Sci. Technol. 17, 1795—1808.
- Wang, Y.J., Jiang, N.J., Han, X.L., Du, Y.J., 2023a. Shear behavior of biochar-amended biocemented calcareous sand treated by biostimulation. Int. J. GeoMech. 23 (1), 04022260.
- Wang, Y.J., Jiang, N.J., Han, X.L., Liu, K., Du, Y.J., 2022. Biochemical, strength and erosional characteristics of coral sand treated by bio-stimulated microbial induced calcite precipitation. Acta Geotech 17 (9), 4217–4229.
- Wang, Y., Jiang, N., Saracho, A.C., Doygun, O., Du, Y., Han, X., 2023b. Compressibility characteristics of bio-cemented calcareous sand treated through the bio-stimulation approach. J. Rock Mech. Geotech. Eng. 15 (2), 510–522.
- Xiao, Y., Wang, Y., Wang, S., Evans, T.M., Stuedlein, A.W., Chu, J., Zhao, C., Wu, H., Liu, H., 2021. Homogeneity and mechanical behaviors of sands improved by a temperature-controlled one-phase MICP method. Acta Geotech 16, 1417–1427.



Dr. Ningjun Jiang is currently a Professor and interim Vice Director of Graduate School at Southeast University (SEU), China. He received his PhD from University of Cambridge, UK. Prior to joining SEU, he was an assistant professor at University of Hawaii at Manoa, USA. His research areas include bio-mediated geotechnics, soil remediation, and ground improvement. Prof. Jiang has published more than 80 journal and conference papers. He has received fundings from National Natural Science Foundation of China, China Ministry of Science and Technology, and Hawaii Department of Transportation. He is the recipient of several academic awards, including Fredlund Award in 2019, Acta Geotechnica Best Paper Award in 2020, Soils and Foundations Editorial Board Member Award in 2021,

and 75th Géotechnique Anniversary Early Career Award in 2023. Prof. Jiang is an Executive Deputy Editor-in-Chief for the journal Biogeotechnics. Previously, he was also an editorial member of Soils and Foundations and Environmental Geotechnics.